EARTH SCIENCES

Intrinsic paleointensity bias and the long-term history of the geodynamo

Aleksey V. Smirnov,[1,2]* Evgeniy V. Kulakov,[3] Marine S. Foucher,[1] Katie E. Bristol[1]

Many geodynamo models predict an inverse relationship between geomagnetic reversal frequency and field strength. However, most of the absolute paleointensity data, obtained predominantly by the Thellier method from bulk volcanic rocks, fail to confirm this relationship. Although low paleointensities are commonly observed during periods of high reversal rate (notably, in the late Jurassic), higher than present-day intensity values are rare during periods of no or few reversals (superchrons). We have identified a fundamental mechanism that results in a pervasive and previously unrecognized low-field bias that affects most paleointensity data in the global database. Our results provide an explanation for the discordance between the experimental data and numerical models, and lend additional support to an inverse relationship between the reversal rate and field strength as a fundamental property of the geodynamo. We demonstrate that the accuracy of future paleointensity analyses can be improved by integration of the Thellier protocol with low-temperature demagnetizations.

INTRODUCTION

The history of Earth's magnetic field, including geomagnetic polarity reversals, secular variation, and field strength variation, is crucial for understanding the geodynamo and planetary evolution. Although the geodynamo could have started as early as during the Hadean (*1*), there has been controversy regarding whether long-term variations of geomagnetic polarity reversals, secular variation, and field strength are intrinsically related or whether they have varied independently throughout geological history. In particular, although a large class of geodynamo models consistently predicts an inverse relationship between geomagnetic reversal frequency and paleointensity (*2*, *3*), to date, most of the paleointensity data—dominated by results from bulk volcanic rocks—fail to confirm this relationship (*4*). Low paleointensity values (40 to 60% of the present-day intensity) are universally recorded during periods of high reversal rate (notably, a portion of the late Jurassic) (*5*–*7*). However, high values that markedly exceed the present-day intensity are rare during periods with no or few reversals (most notably, the Cretaceous Normal Polarity Superchron) (*4*, *8*). This discrepancy suggests either that the numerical models are not accurately describing geodynamo behavior or that there is a pervasive and unrecognized bias in the experimental data that accounts for the absence of high paleointensity values.

The vast majority of absolute paleointensity data have been obtained using the double-heating Thellier method, in which the natural remanent magnetization (NRM) of a sample is gradually replaced with a thermal remanent magnetization (TRM) induced in a known magnetic field in a series of paired heating steps (*9*, *10*). The data points corresponding to each temperature step are evaluated using an NRM-remaining versus a partial TRM (pTRM)–gained plot [Arai plot (*11*)], and the paleointensity is calculated from the slope of a linear segment, corresponding to the unblocking temperature range of the primary remanent magnetization. A fundamental requirement of the Thellier method is that the paleointensity signal is carried by single-domain (SD) magnetic grains that obey the Thellier laws of reciprocity, independence, and additivity (*12*). For these ideal grains, the Arai plot is perfectly linear and yields an accurate estimate of the paleofield strength (*13*). However, rocks used in paleointensity analyses practically always contain larger magnetic grains in the pseudo-SD (PSD) and/or multidomain (MD) states for which the Thellier laws do not hold (*14*). Thellier experiments on these rocks typically result in nonlinear Arai plots (*15*, *16*). However, notwithstanding this limitation, most published syntheses of geodynamo and Earth's interior processes treat paleointensity data from these nonideal carriers as representative of the true paleofield strength [for example, see the study of Biggin *et al.* (*17*)].

Here, we scrutinize the fidelity of rocks containing nonideal magnetic grains as paleointensity recorders by presenting a systematic paleointensity and rock magnetic investigation of synthetic magnetite-bearing samples with a broad range of grain sizes that represent the SD, PSD, and MD magnetic domain states. Paleointensity experiments were conducted using two methods: the double-heating Thellier method, as modified by Coe (*10*) and Coe *et al.* (*18*) (hereafter referred to as the conventional Thellier method), and the low-temperature demagnetization Thellier (LTD-Thellier) method (see Materials and Methods) (*19*).

RESULTS

Rock magnetism

Rock magnetic and paleointensity experiments were conducted on 24 synthetic samples grouped into eight series of three samples each. Samples of the M0.35, M0.75, M1.5, M5, M12, M30, and M250 series contained nearly stoichiometric magnetite powders with grain size modes of 0.35 (acicular), 0.75, 1.5, 5, 12, 30, and 250 μm, respectively (see Materials and Methods). Samples of the MIX series contained a mixture of the ~250-μm magnetite (70%) with the acicular magnetite (30%).

Temperature dependences of low-field magnetic susceptibility [$\kappa(T)$] measured for each series reveal the presence of a single magnetic phase with a Curie temperature of ~585° to 590°C, which is consistent with nearly pure magnetite (fig. S1). A characteristic peak observed at ~153°C (~120 K), associated with the Verwey transition (*20*), indicates that the magnetite is nearly stoichiometric (fig. S1). All $\kappa(T)$ curves are reversible, which confirms the thermal stability of our samples. In addition, after completion of paleointensity experiments, $\kappa(T)$ curves

[1]Department of Geological and Mining Engineering and Sciences, Michigan Technological University, 1400 Townsend Drive, Houghton, MI 49931, USA. [2]Department of Physics, Michigan Technological University, Houghton, MI 49931, USA. [3]Centre for Earth Evolution and Dynamics, University of Oslo, N-0315 Oslo, Norway.
*Corresponding author. Email: asmirnov@mtu.edu

were measured from one of the used samples. All measured curves are similar to those obtained from fresh specimens, which indicates that no magneto-mineralogical alteration occurred during the Thellier experiments.

Magnetic hysteresis loops measured for each series have normal shapes (fig. S2, A to C). The M0.35 samples plot close to the SD region of the Day plot (fig. S2D) (*21*). Although acicular magnetite grains in these samples are larger than the SD threshold for equidimensional magnetite [0.05 to 0.06 μm (*22*)], their nearly SD state is defined by the dominant role of shape anisotropy in the elongate particles (*23*). The M0.75, M1.5, M5, M12, M30, and MIX series have PSD characteristics, plotting along SD-MD mixing lines (*24*) toward the MD region of the Day plot with increasing grain size (fig. S2D). The M250 series has typical MD characteristics (fig. S2D and Table 1). No anisotropy of magnetic hysteresis properties was observed.

In addition, one specimen from each series was placed in a ceramic nonmagnetic boat and heated together with the samples used for paleointensity determinations during conventional Thellier and LTD-Thellier experiments. Magnetic hysteresis parameters for these specimens after completion of paleointensity experiments were indistinguishable from those measured initially, which further attests to the thermal stability of our samples.

No anisotropy of TRM was observed for any series. The TRMs imparted in three orthogonal directions were indistinguishable within experimental errors.

Paleointensity experiments

Before paleointensity experiments were conducted, we modeled the NRM in each sample with a full TRM imparted by cooling from 700°C (in nitrogen) in a 50-μT magnetic field (H_{NRM}). All measured samples yielded interpretable data in both conventional Thellier and LTD-Thellier experiments. For all samples, the full TRM imparted after the final in-field heating step (595°C) was within 3% of the initially imparted TRM, which further attests to their thermal stability. Paleointensity values were calculated by fitting both high-temperature (typically, 525° to 585°C) and low-temperature (100° to 450°C) segments on the Arai plot (Table 1 and tables S1 and S2). Unless stated otherwise, paleointensity values cited below were obtained by fitting high-temperature Arai segments.

Both conventional Thellier and LTD-Thellier experiments on the M0.35 samples resulted in almost ideal, linear Arai plots (Fig. 1), consistent with their nearly SD magnetic state. Slight deviation from linearity at low temperatures most likely reflects the presence of a small amount of equidimensional magnetite in PSD grains. The series-mean paleointensity values are statistically indistinguishable from one another and from H_{NRM} (Table 1).

For all other sample series, the conventional Thellier experiments resulted in concave-up (double-slope) Arai plots, where curvature increased with magnetic grain size (Fig. 2). Mean paleointensity values underestimated H_{NRM} by ~8 to 58% (Table 1). The MIX samples yielded Arai plots similar to those obtained from the M1.5 and M0.75 samples (Fig. 3), with the mean paleointensity underestimating H_{NRM} by ~10%. For all series, mean paleointensity values calculated from low-temperature Arai segments significantly overestimated H_{NRM} by 16 to 280%, with a larger within-series scatter (Table 1).

In LTD-Thellier paleointensity experiments yielded less curved Arai plots compared to their conventional Thellier counterparts for all sample series except for M250. However, the linearization effect strongly depended on magnetic grain size. The M0.75 and M1.5

Table 1. Summary of paleointensity results obtained using the conventional Thellier and LTD-Thellier methods. M_{rs}/M_s is the ratio of saturation remanence to saturation magnetization. "HT fit" and "LT fit" denote the paleofield values (H) calculated by fitting high- and low-temperature segments of the Arai plot, respectively (see text). ΔH is the standard deviation.

Sample	M_{rs}/M_s	Conventional Thellier		LTD-Thellier	
		HT fit $H \pm \Delta H$ (μT)	LT fit $H \pm \Delta H$ (μT)	HT fit $H \pm \Delta H$ (μT)	LT fit $H \pm \Delta H$ (μT)
M0.35-1	0.375	48.8 ± 0.3	61.1 ± 2.2	49.3 ± 0.3	55.2 ± 2.4
M0.35-2	0.384	49.0 ± 0.3	56.1 ± 3.5	49.7 ± 0.2	53.0 ± 1.9
M0.35-3	0.367	49.7 ± 0.1	56.7 ± 5.3	50.1 ± 0.1	50.2 ± 0.1
SD mean	0.375	49.2 ± 0.5	58.0 ± 2.7	49.7 ± 0.4	52.8 ± 2.5
M0.75-1	0.192	46.0 ± 0.2	87.5 ± 3.3	50.3 ± 0.2	57.9 ± 2.9
M0.75-2	0.193	45.0 ± 0.2	91.2 ± 4.8	49.9 ± 0.2	51.5 ± 3.6
M0.75-3	0.182	46.4 ± 1.3	70.2 ± 10.4	49.5 ± 0.6	59.4 ± 5.8
M0.75 mean	0.189	45.8 ± 0.7	83.0 ± 11.2	49.9 ± 0.4	56.3 ± 4.2
M1.5-1	0.151	44.0 ± 0.1	107.3 ± 11.1	49.1 ± 0.1	54.6 ± 3.8
M1.5-2	0.149	44.1 ± 0.4	99.3 ± 6.8	49.5 ± 0.6	52.8 ± 5.2
M1.5-3	0.139	43.4 ± 0.9	105.7 ± 11.5	48.6 ± 0.4	61.1 ± 3.6
M1.5 mean	0.146	43.8 ± 0.4	104.1 ± 4.2	49.1 ± 0.5	56.2 ± 4.4
M5-1	0.105	40.5 ± 0.8	117.1 ± 7.5	48.3 ± 0.3	62.9 ± 2.3
M5-2	0.113	39.8 ± 1.1	121.7 ± 8.2	47.0 ± 0.5	75.9 ± 8.0
M5-3	0.110	38.9 ± 1.3	143.0 ± 11.5	47.8 ± 0.4	68.9 ± 6.1
M5 mean	0.109	39.7 ± 0.8	127.3 ± 13.8	47.7 ± 0.7	69.2 ± 6.5
M12-1	0.074	35.2 ± 1.5	145.2 ± 14.2	45.2 ± 0.8	80.9 ± 12.7
M12-2	0.076	35.8 ± 0.6	104.7 ± 11.1	44.5 ± 0.9	82.2 ± 6.0
M12-3	0.077	36.6 ± 1.7	137.7 ± 13.6	45.0 ± 0.4	73.8 ± 3.0
M12 mean	0.076	35.8 ± 0.7	129.2 ± 21.6	44.9 ± 0.4	79.0 ± 4.5
M30-1	0.048	28.2 ± 1.2	116.3 ± 12.2	34.3 ± 1.6	136.3 ± 5.3
M30-2	0.046	28.5 ± 2.0	139.3 ± 8.2	33.7 ± 1.8	122.5 ± 3.6
M30-3	0.043	29.4 ± 1.9	132.3 ± 7.6	35.0 ± 1.6	110.4 ± 3.0
M30 mean	0.046	28.7 ± 0.6	129.3 ± 11.8	34.3 ± 0.7	123.1 ± 13.0
M250-1	0.024	20.7 ± 1.6	184.7 ± 15.6	21.9 ± 1.3	157.5 ± 12.6
M250-2	0.025	21.0 ± 1.8	180.7 ±15.4	22.1 ± 1.4	159.5 ± 10.6
M250-3	0.024	21.2 ± 2.2	206.9 ± 8.8	22.8 ± 2.0	173.4 ± 6.4
M250 mean	0.024	21.0 ± 0.3	190.7 ± 14.1	22.3 ± 0.5	163.5 ± 8.7
MIX-1	0.131	43.1 ± 1.4	104.4 ± 6.2	47.8 ± 0.6	72.7 ± 3.9
MIX-2	0.125	44.7 ± 1.0	92.6 ± 6.2	48.3 ± 0.4	66.2 ± 1.9
MIX-3	0.135	45.3 ± 0.9	87.6 ± 5.6	48.7 ± 0.3	103.3 ± 5.1
MIX mean	0.130	44.4 ± 1.1	94.8 ± 8.6	48.3 ± 0.4	80.7 ± 19.8

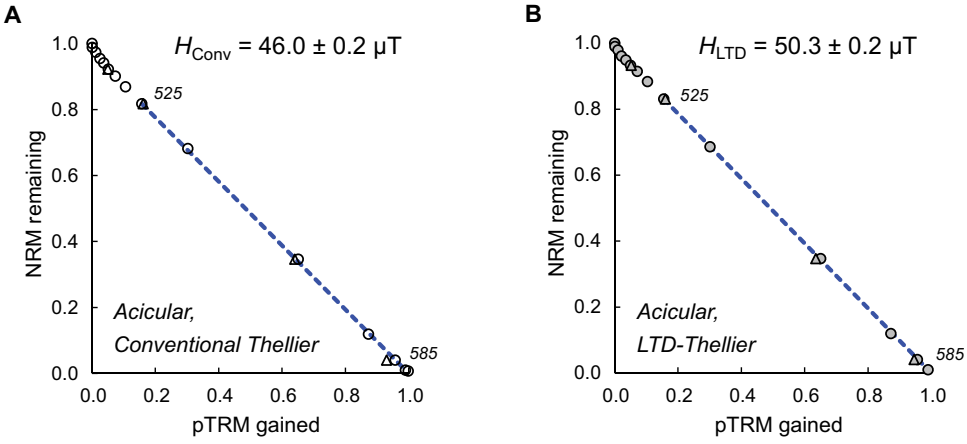

Fig. 1. Examples of paleointensity determinations from an M0.35 sample containing acicular (SD) magnetite. Data are obtained using the conventional Thellier (**A**) and LTD-Thellier (**B**) methods. NRM remaining versus pTRM gained (circles) is shown. Triangles are pTRM checks. The blue dashed line is the best-fit line for a high-temperature Arai segment used to calculate paleointensity estimates H_{Conv} (A) and H_{LTD} (B) (the numbers in italics indicate the temperature range, in degrees Celsius). The best-fit lines for low-temperature Arai segments are not shown for clarity.

samples yielded nearly linear Arai plots (Fig. 2, A and B) and mean paleointensity values that accurately reproduce H_{NRM} (Table 1). The M5 samples resulted in slightly curved Arai plots (Fig. 2C), with mean paleointensity within 5% of H_{NRM}. We note that Xu and Dunlop (*16*) did not observe improved linearity of LTD-Thellier Arai plots for a sample containing ~6-μm magnetite grains. Although the reason for this discrepancy remains unclear, we speculate that it may reflect inefficient LTD in the previous study due to sample oxidation. The M12 samples gave rise to double-sloped Arai plots (Fig. 2D), with mean paleointensity within ~10% of H_{NRM}. Similarly, the MIX series yielded a mean paleointensity that underestimates H_{NRM} by 3 to 4% (Fig. 3 and Table 1).

The linearization effect of the LTD-Thellier method was much less expressed for the M30 series (Fig. 2E), which produced a mean paleointensity value that significantly (by 31%) underestimates H_{NRM}, albeit to a lesser extent than the conventional Thellier method (Table 1). For the M250 series, the LTD-Thellier method did not result in significant improvement of the Arai plot linearity compared with conventional Thellier data (Fig. 2F). The corresponding mean paleointensity underestimated the true field by ~55% (Table 1). These results are consistent with behavior observed for MD magnetite in previous studies (*13*, *16*).

For all measured samples, the low-temperature segments of LTD-Thellier Arai plots are, on average, shallower than their conventional counterparts (Figs. 2 and 3). Nevertheless, corresponding mean paleointensity values overestimated H_{NRM} by 6 to 226% (Table 1).

DISCUSSION

Most absolute paleointensity data have been obtained using variants of the conventional Thellier method from rocks containing PSD magnetic grains, with saturation remanence to saturation magnetization (M_{rs}/M_s) ratios as low as 0.1 [for example, see the study of Zhu *et al.* (*8*)]. Our results demonstrate that these nonideal Thellier experiments may underestimate the true paleofield strength by as much as 25% (Table 1 and Fig. 4). We note that, although curvature of Arai plots and attendant bias may be reduced when the directions of NRM and laboratory magnetic field H_{lab} are not parallel, nonlinear Arai plots have been observed even in perpendicular Thellier experiments [for example, see the study of Xu and Dunlop (*16*)]. Because intrinsic low-field bias is fully controlled by magnetic domain state, it should affect all nonideal data independent of the magnetic mineralogy of studied rocks.

Pervasive bias due to the presence of nonideal carriers of paleointensity signal identified by our analyses represents a fundamental physical mechanism that contributes to the dominance of low virtual dipole moment values in the global paleointensity database. In some cases, this bias can be compounded by several additional mechanisms, such as experimental alteration of basalts (*25*) and basaltic glass (*26*), low-temperature oxidation, and hydrothermal alteration (*27*). These factors are likely to account for the deficit of paleointensity values exceeding the present-day value (~8×10^{22} Am^2) observed from bulk rock data during the Cretaceous Normal Polarity and the Kiaman Reversed Polarity Superchrons [for example, see the studies of Zhu *et al.* (*8*) and Garcia *et al.* (*28*)]. Therefore, our results provide a feasible explanation for the apparent discordance between experimental data based on whole rock analyses and numerical models, and lend additional credibility to an inverse relationship between geomagnetic reversal rate and field strength. This interpretation is further corroborated by high-fidelity paleointensity data from single silicate crystals that contain SD magnetic inclusions (*29*), which consistently indicate high field strengths (12.5×10^{22} to 12.7×10^{22} Am^2) during superchrons (*30*–*32*) and low field strengths (4.1×10^{22} to 5.2×10^{22} Am^2) during periods of high reversal frequency, such as the late Jurassic (*5*).

An important corollary of our investigation is that statistical treatments of the global paleomagnetic database from bulk rock samples may not truly represent the long-term behavior of the field strength. Consequently, our data call into question the veracity of some long-term features of the field, such as the Mesozoic Dipole Low (MDL) (*33*). The MDL was originally proposed on the basis of Thellier analyses of bulk rocks, which suggested geomagnetic field strengths much lower than those of the present day. However, our results support a contrasting view that the apparent low field strength during the MDL may reflect a low-field bias due to rock magnetic effects, and, instead, that the real "MDL" is reduced to an interval of high reversal frequency in the late Jurassic at ~150 to 170 million years ago (*5*, *34*).

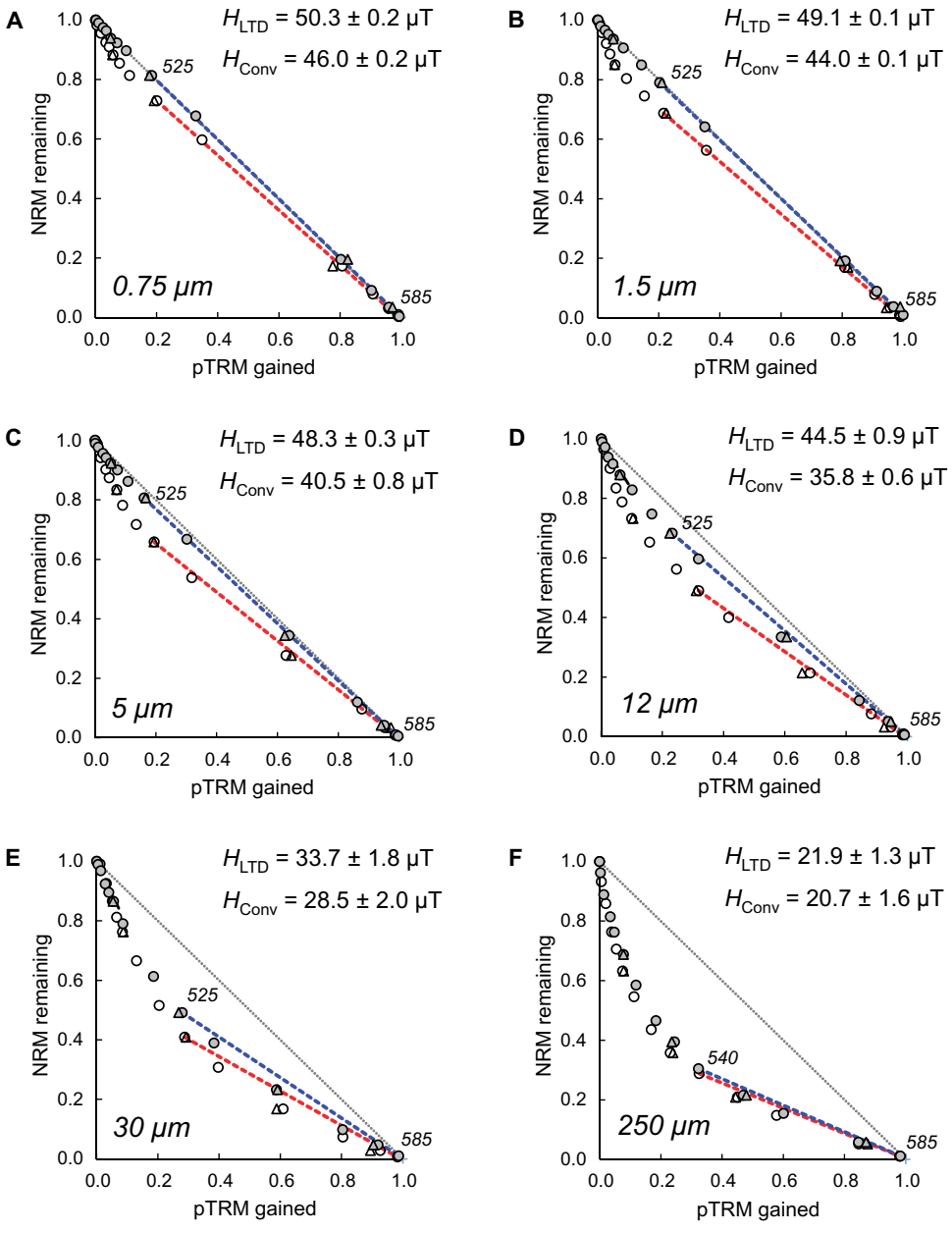

Fig. 2. Examples of Thellier paleointensity determinations. Data from series M0.75 (**A**), M1.5 (**B**), M5 (**C**), M12 (**D**), M30 (**E**), and M250 (**F**). NRM remaining versus pTRM gained (circles) is shown. Open and closed symbols represent data measured using the conventional Thellier and LTD-Thellier methods, respectively. Triangles are pTRM checks. Red and blue dashed lines are the best-fit lines for high-temperature Arai segments (the numbers in italics indicate the corresponding temperature range, in degrees Celsius) used to calculate paleointensity estimates H_{Conv} and H_{LTD} for the conventional Thellier and LTD-Thellier methods, respectively. The best-fit lines for low-temperature Arai segments are not shown for clarity. The negative unit slope line (dotted line) represents the ideal paleointensity behavior expected for an ideal SD carrier (see text).

Similarly, with pervasive fundamental low-field paleointensity bias, some other inferences about long-term geodynamo features, such as the "Proterozoic Dipole Low" (*35*) or a consistently low long-term global average axial dipole magnetic moment [for example, see the study of Wang *et al.* (*36*)], require additional scrutiny and may need to be revised. A thorough analysis of the original paleointensity publications is required to determine the extent to which the data are affected by the low-field bias.

Our experimental analyses also demonstrate that, in addition to low-field bias, nonideal Thellier experiments substantially overestimate the true paleofield strength if the low-temperature segment of a double-slope Arai plot is used for best-line fitting, even for PSD samples containing relatively small (0.5 to 1.5 μm) grains (Table 1). Thus, our study corroborates conclusions of previous studies [for example, see the study of Shcherbakov and Shcherbakova (*15*)] that these paleointensity values should not be accepted as a faithful paleofield estimate. Nevertheless, data affected by such a high-field bias [for example, see the study of Thomas and Piper (*37*)] have been included in the global paleointensity database; noncritical acceptance of these

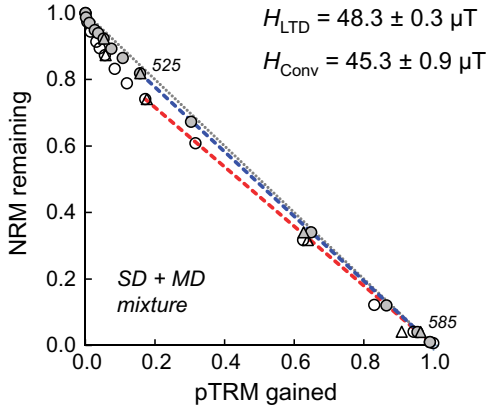

Fig. 3. An example of Thellier paleointensity determinations from the MIX series. NRM remaining versus pTRM gained. Open and closed symbols indicate the data measured using the conventional Thellier and LTD-Thellier methods, respectively. Triangles are pTRM checks. Red and blue dashed lines are the best-fit lines for high-temperature Arai segments (the numbers in italics indicate the corresponding temperature range, in degrees Celsius) used to calculate paleointensity estimates H_{Conv} and H_{LTD} for the conventional Thellier and LTD-Thellier methods, respectively. The best-fit lines for low-temperature Arai segments are not shown for clarity. The negative unit slope line (dotted line) represents the ideal paleointensity behavior expected for an ideal SD carrier (see text).

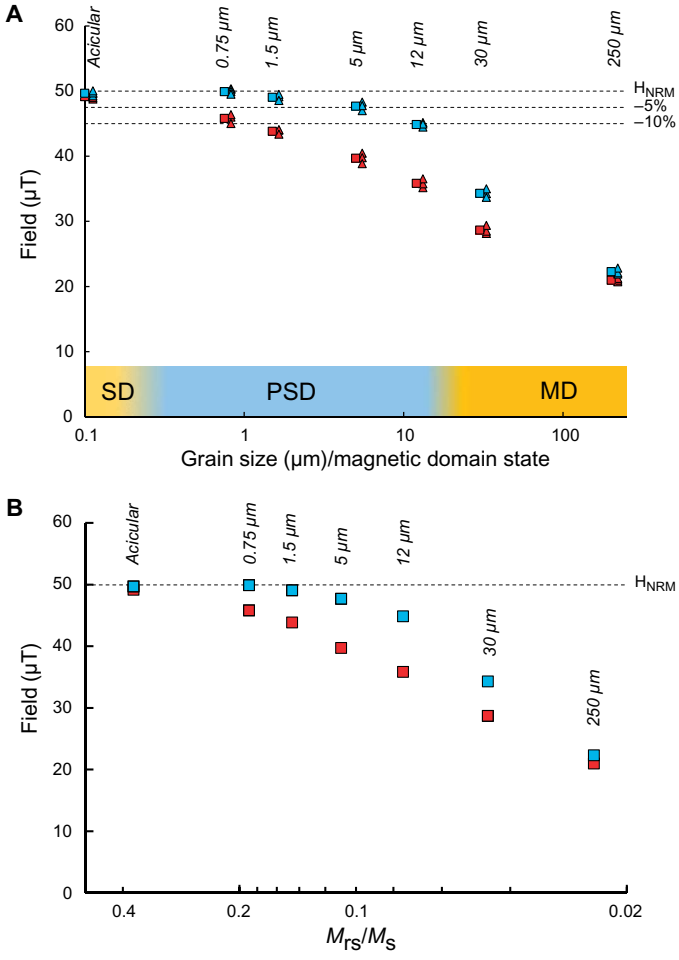

Fig. 4. Summary of paleointensity results. Red and light blue symbols represent data obtained using the conventional Thellier and LTD-Thellier methods, respectively. (**A**) Grain size/magnetic domain state dependence. Triangles, data for individual samples (tables S1 and S2); squares, mean paleointensity values (Table 1). The 0.1-μm grain size used for the M0.35 (acicular magnetite) sample is arbitrary. Individual data points are shifted with respect to the mean for clarity. Horizontal dashed lines correspond to the field of initial NRM acquisition (H_{NRM} = 50 μT) and to the 5 and 10% underestimate levels of H_{NRM}. (**B**) Mean paleointensity values versus the mean M_{rs}/M_s (saturation remanence to saturation magnetization) ratios (Table 1).

data can lead to artifacts in reconstructing geodynamo history and in estimating the age of inner core (*38*).

Although it is virtually impossible to correct existing data for bias due to nonideal magnetic carriers and other factors, all possible efforts should be made to obtain more accurate determinations in new paleointensity experiments. Our investigation contributes to these efforts by demonstrating that integration of the conventional Thellier approach with LTD-Thellier represents an efficient tool to improve the accuracy of paleointensity determinations by eliminating or significantly reducing intrinsic bias in samples containing PSD magnetite (<10-μm grain size). Furthermore, our data from the MIX series indicate that the LTD-Thellier method may also produce more accurate results from rocks containing two distinct populations of magnetite grains (for example, large magnetite phenocrysts and submicrometer magnetite inclusions in silicate crystals). Although the LTD-Thellier method is only effective for magnetite-bearing rocks, nearly stoichiometric PSD magnetite [for example, formed by subsolidus reactions during initial cooling (*39*)] represents the most common remanence carrier in both extrusive and intrusive igneous rocks used for paleointensity investigations. The LTD behavior of natural samples may differ to some extent from that of our synthetic samples, due to the pinning of domain walls at exsolution phase boundaries and/or crystalline lattice defects; however, the intrinsic paleointensity bias is unlikely to be significantly affected by these mechanisms (*40*). All studies using the LTD-Thellier method, albeit limited in number, have resulted in higher success rates and increased quality of paleointensity results (*41*–*43*).

Complete understanding of the physical mechanisms responsible for the efficiency of the LTD-Thellier approach awaits development of a comprehensive theory of both thermal remanence and LTD in PSD and MD magnetite. The LTD-Thellier method was originally proposed on the basis of the notion that LTD preferentially removes less stable remanence components carried by MD magnetite and, thus, should magnify the paleointensity signal carried by SD grains and/or SD-like structures in larger grains [for example, see the study of Schmidt (*19*)]. Although the fraction of remanence removed by LTD in our experiments was increasingly larger for samples containing larger size grains, reaching a maximum for MD samples, the linearization effect of the LTD-Thellier approach was most strongly expressed for our PSD samples and is practically absent for MD samples (Table 1). We suggest that this dichotomy may reflect the inherent difference between PSD and MD magnetite in the relative effect of crystallographic twinning (*44*) or thermal activation of magnetic vortices (*45*) in monoclinic magnetite on the LTD process.

MATERIALS AND METHODS

Sample preparation

For our synthetic samples, we used six different magnetite powders characterized by log-normal grain size distributions with modes of 0.35, 0.75,

1.5, 5, 12, and 30 μm. The 0.35-μm powder contained acicular grains with aspect ratios ranging from ~1:6 to 1:12, whereas magnetite grains in the five other powders have an irregular, nearly equidimensional shape (*46*). An additional powder, prepared by crushing natural magnetite crystals, had a grain size ranging from 100 to 400 μm with a mode of ~250 μm. To obtain nearly stoichiometric magnetite, we reduced the powders in a CO_2/CO (9:1) atmosphere at 400°C for 4 hours. Temperature dependence of low-field magnetic susceptibility measured from the reduced powders upon cycling to 700°C in argon was reversible and revealed the presence of a single magnetic phase with Curie temperatures of ~585° to 590°C, which is consistent with nearly pure magnetite.

To prepare samples for paleointensity experiments, we thoroughly mixed the reduced magnetite powders with dry CaF_2 powder and added a minute amount of distilled water to the mixtures to produce a dense paste. Next, 1-cm^3 cubes were made out of the paste, which was air-dried for 24 hours; after which, the drying process was completed by gradually heating the samples to 400°C (in nitrogen) for 5 hours. Three samples were prepared from each magnetite powder (referred to as the M0.35, M0.75, M1.5, M5, M12, and M30 series). An additional set of three samples (the M250 series) was prepared using the crushed natural magnetite powder. Finally, three samples (the MIX series) containing a mixture of ~250-μm magnetite (70%) with acicular magnetite (30%) were prepared. The same procedure was used to create additional samples for rock magnetic experiments.

Rock magnetism

Magnetic hysteresis parameters (coercivity, H_c; coercivity of remanence, H_{cr}; saturation remanence, M_{rs}; and saturation magnetization, M_s) were measured at room temperature using an alternating gradient magnetometer (AGM) (model 2900, Princeton Measurement Corporation). The maximum applied field of 0.5 T was used for both magnetic hysteresis loop and backfield demagnetization curve measurements. To test for magnetic anisotropy, we rotated samples (45° increments) on parallel and perpendicular AGM stages, and measured magnetic hysteresis parameters after each rotation.

Temperature dependences of low-field magnetic susceptibility, $\kappa(T)$, were measured upon cycling the samples from room temperature to 700°C (in argon) using an AGICO MFK-1FA magnetic susceptibility meter equipped with a high-temperature furnace and cryostat. The $\kappa(T)$ curves were also measured upon heating from ~192°C (~180 K) to room temperature before and after the high-temperature thermomagnetic runs. The field applied in all $\kappa(T)$ experiments was 200 A/m.

To test for anisotropy of TRM, we compared the magnitudes of TRMs imparted in a cubic sample from each series in three mutually orthogonal directions. TRMs were imparted by cooling samples from 700°C (in nitrogen) in a 50-μT field using a thermal specimen demagnetizer (model TD-48SC, ASC Scientific).

Thellier paleointensity experiments

Conventional Thellier experiments followed the Thellier protocol modified by Coe (*10*) and Coe *et al.* (*18*). Zero-field and in-field heatings were done in a thermal specimen demagnetizer (model TD-48SC, ASC Scientific) in an inert (99.9% nitrogen) atmosphere. For the in-field steps, the laboratory magnetic field (H_{lab} = 50 μT) was applied parallel to the NRM direction. Samples were always placed at exactly the same position and orientation in the thermal demagnetizer. The temperature steps at 100°, 200°, 300°, 350°, 400°, 450°, 500°, 525°, 540°, 555°, 565°, 575°, 585°, and 595°C were used. To monitor for experimental alteration, we performed four pTRM checks at 400°, 525°, 555°, and 575°C. The pTRM checks were judged to be successful if they fell within 5% of the original pTRM value. In both conventional Thellier and LTD-Thellier experiments, the magnetic remanence was measured using a 2G Enterprises 760-R superconducting rock magnetometer located in a magnetically shielded laboratory. The resulting paleointensity data were processed using the ThellierTool-4.22 software (*47*).

LTD-Thellier experiments followed the same protocol as described above except that samples were subjected to two successive LTD steps after each heating. The LTD was conducted by immersing samples in liquid nitrogen in a magnetic field–free environment. The samples warmed to room temperature at a natural rate (no forced heating was applied). The number of LTD treatments needed for effective demagnetization of MD-like remanences was determined experimentally by applying several LTDs to a laboratory TRM induced in a 50-μT field. For all sample series, the difference in remanence measured after the second and third LTD did not exceed 1%. The remanence directions before and after LTDs were indistinguishable.

SUPPLEMENTARY MATERIALS

Supplementary material for this article is available at http://advances.sciencemag.org/cgi/content/full/3/2/e1602306/DC1

Supplementary Results

fig. S1. Typical dependences of low-field magnetic susceptibility versus temperature.

fig. S2. Magnetic hysteresis properties.

table S1. Paleointensity results obtained using the conventional Thellier method by fitting the high- and low-temperature segments of the Arai plots.

table S2. Paleointensity results obtained using the LTD-Thellier method by fitting the high- and low-temperature segments of the Arai plots.

REFERENCES AND NOTES

1. J. A. Tarduno, R. D. Cottrell, W. J. Davis, F. Nimmo, R. K. Bono, A Hadean to Paleoarchean geodynamo recorded by single zircon crystals. *Science* **349**, 521–524 (2015).
2. P. Driscoll, P. Olson, Effects of buoyancy and rotation on the polarity reversal frequency of gravitationally driven numerical dynamos. *Geophys. J. Int.* **178**, 1337–1350 (2009).
3. J. Aubert, J. A. Tarduno, C. L. Johnson, Observations and models of the long-term evolution of Earth's magnetic field. *Space Sci. Rev.* **155**, 337–370 (2010).
4. E. Ingham, D. Heslop, A. P. Roberts, R. Hawkins, M. Sambridge, Is there a link between geomagnetic reversal frequency and paleointensity? A Bayesian approach. *J. Geophys. Res.* **119**, 5290–5304 (2014).
5. J. A. Tarduno, R. D. Cottrell, Dipole strength and variation of the time-averaged reversing and non-reversing geodynamo based on Thellier analyses of single plagioclase crystals. *J. Geophys. Res.* **110**, B11101 (2005).
6. L. Tauxe, J. S. Gee, M. B. Steiner, H. Staudigel, Paleointensity results from the Jurassic: New constraints from submarine basaltic glasses of ODP Site 801C. *Geochem. Geophys. Geosyst.* **14**, 4718–4733 (2013).
7. C. J. Sprain, J. M. Feinberg, J. W. Geissman, B. Strauss, M. C. Brown, Paleointensity during periods of rapid reversal: A case study from the Middle Jurassic Shamrock batholith, western Nevada. *Geol. Soc. Am. Bull.* **128**, 223–238 (2016).
8. R. Zhu, Y. Pan, H. He, H. Qin, S. Ren, Paleomagnetism and $^{40}Ar/^{39}Ar$ age from a Cretaceous volcanic sequence, Inner Mongolia, China: Implications for the field variation during the Cretaceous normal superchron. *Phys. Earth Planet. Inter.* **169**, 59–75 (2008).
9. E. Thellier, O. Thellier, Sur l'intensité du champ magnétique terrestre dans le passé historique et géologique. *Ann. Geophys.* **15**, 285–378 (1959).
10. R. S. Coe, Paleo-intensities of Earth's magnetic field determined from Tertiary and Quaternary Rocks. *J. Geophys. Res.* **72**, 3247–3262 (1967).
11. T. Nagata, Y. Arai, K. Momose, Secular variation of the geomagnetic total force during the last 5000 years. *J. Geophys. Res.* **68**, 5277–5281 (1963).
12. E. Thellier, O. Thellier, Sur les variations thermiques de l'aimantation thermorémanente des terres cuites. *C. R. Acad. Sci.* **213**, 59–61 (1941).
13. D. J. Dunlop, B. Zhang, Ö. Özdemir, Linear and nonlinear Thellier paleointensity behavior of natural minerals. *J. Geophys. Res.* **110**, 1–15 (2005).
14. V. A. Shashkanov, V. V. Metallova, Violation of Thellier's law for partial thermoremanent magnetization. *Izv. Acad. Sci. USSR Phys. Solid Earth* **8**, 180–184 (1972).

15. V. P. Shcherbakov, V. V. Shcherbakova, On the suitability of the Thellier method of palaeointensity determinations on pseudo-single-domain and multidomain grains. *Geophys. J. Int.* **146**, 20–30 (2001).
16. S. Xu, D. J. Dunlop, Thellier paleointensity theory and experiments for multidomain grains. *J. Geophys. Res.* **109**, B07103 (2004).
17. A. J. Biggin, B. Steinberger, J. Aubert, N. Suttie, R. Holme, T. H. Torsvik, D. G. van der Meer, D. J. J. van Hinsbergen, Possible links between long-term geomagnetic variations and whole-mantle convection processes. *Nat. Geosci.* **5**, 526–533 (2012).
18. R. S. Coe, S. Grommé, E. A. Mankinen, Geomagnetic paleointensities from radiocarbon dated lava flows on Hawaii and the question of the Pacific nondipole low. *J. Geophys. Res.* **83**, 1740–1756 (1978).
19. P. W. Schmidt, Paleomagnetic cleaning strategies. *Phys. Earth Planet. Inter.* **76**, 169–178 (1993).
20. E. J. W. Verwey, Electronic conduction of magnetite (Fe3O4) and its transition point at low temperatures. *Nature* **44**, 327–328 (1939).
21. R. Day, M. Fuller, V. A. Schmidt, Hysteresis properties of titanomagnetites: Grain-size and composition dependence. *Phys. Earth Planet. Inter.* **13**, 260–267 (1977).
22. D. J. Dunlop, Ö. Özdemir, *Rock Magnetism, Fundamentals and Frontiers* (Cambridge Univ. Press, 1997), p. 557.
23. R. F. Butler, S. K. Banerjee, Theoretical single-domain grain-size range in magnetite and titanomagnetite. *J. Geophys. Res.* **80**, 4049–4058 (1975).
24. D. J. Dunlop, Theory and application of the Day plot (M_{rs}/M_s versus H_{cr}/H_c) 1. Theoretical curves and tests using titanomagnetite data. *J. Geophys. Res.* **107**, EPM 4-1–EPM 4-22 (2002).
25. R. D. Cottrell, J. A. Tarduno, In search of high fidelity geomagnetic paleointensities: A comparison of single plagioclase crystal and whole rock Thellier-Thellier analyses. *J. Geophys. Res.* **105**, 23579–23594 (2000).
26. A. V. Smirnov, J. A. Tarduno, Magnetic hysteresis monitoring of Cretaceous submarine basaltic glass during Thellier paleointensity experiments: Evidence for alteration and attendant low field bias. *Earth Planet. Sci. Lett.* **206**, 571–585 (2003).
27. J. A. Tarduno, A. V. Smirnov, The paradox of low field values and the long-term history of the geodynamo, in *Timescales of the Paleomagnetic Field*, J. E. T. Channell, D. V. Kent, W. Lowrie, J. G. Meert, Eds. (American Geophysical Union, 2004).
28. A. S. Garcia, D. N. Thomas, D. Liss, J. Shaw, Low geomagnetic field intensity during the Kiaman superchron: Thellier and microwave results from the Great Whin Sill intrusive complex, northern United Kingdom. *Geophys. Res. Lett.* **33**, L16308 (2006).
29. J. A. Tarduno, R. D. Cottrell, A. V. Smirnov, The paleomagnetism of single silicate crystals: Recording geomagnetic field strength during mixed polarity intervals, superchrons, and inner core growth. *Rev. Geophys.* **44**, RG1002 (2006).
30. J. A. Tarduno, R. D. Cottrell, A. V. Smirnov, High geomagnetic field intensity during the mid-Cretaceous from Thellier analyses of single plagioclase crystals. *Science* **291**, 1779–1783 (2001).
31. J. A. Tarduno, R. D. Cottrell, A. V. Smirnov, The Cretaceous superchron geodynamo: Observations near the tangent cylinder. *Proc. Natl. Acad. Sci. U.S.A.* **99**, 14020–14025 (2002).
32. R. D. Cottrell, J. A. Tarduno, J. Roberts, The Kiaman Reversed Polarity Superchron at Kiama: Toward a field strength estimate based on single silicate crystals. *Phys. Earth Planet. Inter.* **169**, 49–58 (2008).
33. M. Prévot, M. E. Derder, M. O. McWilliams, J. Thompson, Intensity of the Earth's magnetic field: Evidence for a Mesozoic dipole low. *Earth Planet. Sci. Lett.* **97**, 129–139 (1990).
34. A. Goguitchaichvili, L. M. Alva-Valdivia, J. Urrutia, J. Morales, O. F. Lopes, On the reliability of Mesozoic Dipole Low: New absolute paleointensity results from Paraná Flood Basalts (Brazil). *Geophys. Res. Lett.* **29**, 33-1–33-4 (2002).
35. A. J. Biggin, G. H. M. A. Strik, C. G. Langereis, The intensity of the geomagnetic field in the late-Archaean: New measurements and an analysis of the upgraded IAGA paleointensity database. *Earth Planets Space* **61**, 9–22 (2009).
36. H. Wang, D. V. Kent, P. Rochette, Weaker axially dipolar time-averaged paleomagnetic field based on multidomain-corrected paleointensities from Galapagos lavas. *Proc. Natl. Acad. Sci. U.S.A.* **112**, 15036–15041 (2015).
37. D. N. Thomas, J. D. A. Piper, Evidence for the existence of a transitional geomagnetic field recorded in a Proterozoic lava succession. *Geophys. J. Int.* **122**, 266–282 (1995).
38. A. V. Smirnov, J. A. Tarduno, E. V. Kulakov, S. A. McEnroe, R. K. Bono, Palaeointensity, core thermal conductivity and the unknown age of the inner core. *Geophys. J. Int.* **205**, 1190–1195 (2016).
39. S. E. Haggerty, Oxide textures; A mini-atlas. *Rev. Mineral. Geochem.* **25**, 129–219 (1991).
40. A. A. Kosterov, Magnetic properties, low-temperature, in *Encyclopedia of Geomagnetism and Paleomagnetism*, D. Gubbins, E. Herrero-Bervera, Eds. (Springer, 2007). pp. 515–525.
41. K. R. Celino, R. I. F. Trindade, E. Tohver, LTD-Thellier paleointensity of 1.2 Ga Nova Floresta mafic rocks (Amazon craton). *Geophys. Res. Lett.* **34**, L12306 (2007).
42. E. V. Kulakov, A. V. Smirnov, J. F. Diehl, Absolute geomagnetic paleointensity as recorded by ~1.09 Ga Lake Shore Traps (Keweenaw Peninsula, Michigan). *Stud. Geophys. Geod.* **57**, 565–584 (2013).
43. A. V. Smirnov, D. A. D. Evans, Geomagnetic paleointensity at ~2.41 Ga as recorded by the Widgiemooltha Dike Swarm, Western Australia. *Earth Planet. Sci. Lett.* **416**, 35–45 (2015).
44. A. V. Smirnov, Low-temperature magnetic properties of magnetite using first-order reversal curve analysis: Implications for the pseudo-single-domain state. *Geochem. Geophys. Geosyst.* **7**, Q11011 (2006).
45. A. R. Muxworthy, W. Williams, Micromagnetic models of pseudo-single domain grains of magnetite near the Verwey Transition. *J. Geophys. Res.* **104**, 29203–29217 (1999).
46. A. V. Smirnov, Memory of the magnetic field applied during cooling in the low-temperature phase of magnetite: Grain size dependence. *J. Geophys. Res.* **111**, B12S04 (2006).
47. R. Leonhardt, C. Heunemann, D. Krása, Analyzing absolute paleointensity determinations: Acceptance criteria and the software ThellierTool4.0. *Geochem. Geophys. Geosyst.* **5**, Q12016 (2004).

Acknowledgments: We thank A. Roberts and two anonymous reviewers for their helpful comments. **Funding:** This work was funded by the NSF. **Author contributions:** A.V.S. and E.V.K. conceived the study. A.V.S. supervised the research. A.V.S. and E.V.K. designed the experiments. A.V.S., E.V.K., M.S.F., and K.E.B. carried out the experiments. A.V.S. led the writing of the paper with contributions from E.V.K., M.S.F., and K.E.B. **Competing interests:** The authors declare that they have no competing interests. **Data and materials availability:** All data needed to evaluate the conclusions in the paper are present in the paper and/or the Supplementary Materials. Additional data related to this paper may be requested from the authors.

Submitted 20 September 2016
Accepted 10 January 2017
Published 15 February 2017
10.1126/sciadv.1602306

Citation: A. V. Smirnov, E. V. Kulakov, M. S. Foucher, K. E. Bristol, Intrinsic paleointensity bias and the long-term history of the geodynamo. *Sci. Adv.* **3**, e1602306 (2017).

Science Advances

Intrinsic paleointensity bias and the long-term history of the geodynamo

Aleksey V. Smirnov, Evgeniy V. Kulakov, Marine S. Foucher and Katie E. Bristol

Sci Adv **3** (2), e1602306.
DOI: 10.1126/sciadv.1602306